


Cite this: *RSC Adv.*, 2025, 15, 513

# An eco-friendly and cost-effective approach for the synthesis of a novel GA@CuO–ZnO nanocomposite: characterization, antimicrobial and anticancer activities

Gharieb S. El-Sayyad,<sup>a</sup> El-Sayed R. El-Sayed,<sup>c</sup> Samar H. Rizk,<sup>d</sup> Mostafa A. Abdel-Maksoud,<sup>e</sup> Adel M. Zakri,<sup>f</sup> Abdul Malik,<sup>g</sup> Mohamed N. Malash<sup>h</sup> and Amr H. Hashem<sup>i</sup>

In this study, a nanocomposite based on copper oxide–zinc oxide nanoparticles and Gum Arabic (GA@CuO–ZnO nanocomposite) was successfully synthesized using green method. Characterization results revealed that the prepared nanocomposite appeared at the nanoscale level, showed excellent dispersion, and formed stable colloidal nano-solutions. The bimetallic GA@CuO–ZnO nanocomposite was evaluated for its anticancer, antibacterial, and antifungal properties. Cytotoxicity testing of the synthesized GA@CuO–ZnO nanocomposite against Wi38 and Vero normal cell lines showed IC<sub>50</sub> values of 143.3 and 220.9  $\mu\text{g ml}^{-1}$ , respectively, indicating that the nanocomposite is safe for use. Moreover, the synthesized GA@CuO–ZnO nanocomposite showed anticancer activity against HepG2 and MCF7 cell lines, with IC<sub>50</sub> values of 54.7 and 79.2  $\mu\text{g ml}^{-1}$ , respectively. The nanocomposite also showed promising antibacterial activity against *Escherichia coli*, *Salmonella typhimurium*, *Staphylococcus aureus*, *S. epidermis*, and *Bacillus subtilis*, with MIC values ranging from 31.25 to 62.5  $\mu\text{g ml}^{-1}$ . Furthermore, the prepared nanocomposite exhibited antifungal activity against *Candida albicans*, *Cryptococcus neoformans*, *Aspergillus fumigatus* and *A. brasiliensis*, with an MIC of 31.25  $\mu\text{g ml}^{-1}$  against all tested fungal strains, except *A. fumigatus* (MIC 125  $\mu\text{g ml}^{-1}$ ). In conclusion, the synthesized GA@CuO–ZnO nanocomposite was successfully synthesized, and it exhibited promising antibacterial, antifungal and anticancer activities at safe doses.

Received 12th June 2024  
Accepted 26th August 2024

DOI: 10.1039/d4ra04312j

rsc.li/rsc-advances

## Introduction

Antimicrobial resistance (AMR) refers to the ability of micro-organisms to develop resistance to medications that were once

effective in treating infections. It represents a significant global health threat as it hampers the efficacy of antimicrobial medications and complicates the treatment of infections. Multiple factors contribute to the emergence of antibiotic resistance.<sup>1</sup> A key factor is the overuse and misuse of antibiotics in human and animal healthcare, as well as in agriculture. Improper or unnecessary use of antibiotics can drive the adaptation and development of resistance mechanisms in bacteria, enabling their survival. The transfer of resistance can occur among several bacterial species via mobile genetic components, exacerbating the problem.<sup>2</sup> Antimicrobial resistance presents substantial obstacles in healthcare, leading to extended and more intricate treatment regimens, elevated healthcare expenses, and higher mortality rates.<sup>3</sup> Infections caused by antibiotic-resistant bacteria are often associated with extended periods of hospitalization and increased rates of treatment failure. Moreover, the development of novel antimicrobial medications is progressing at a slower rate than the rapid emergence of resistance, underscoring the urgent need for responsible and judicious use of antimicrobial agents.<sup>4</sup>

Cancer is a multifaceted collection of illnesses distinguished by the unregulated proliferation and dissemination of aberrant cells. These cells possess the capacity to infiltrate and destroy

<sup>a</sup>Medical Laboratory Technology Department, Faculty of Applied Health Sciences Technology, Badr University in Cairo (BUC), Badr city, Cairo 11829, Egypt. E-mail: Gharieb.El-Saied@buc.edu.eg

<sup>b</sup>Drug Microbiology Lab, Drug Radiation Research Department, National Center for Radiation Research and Technology (NCRRT), Egyptian Atomic Energy Authority (EAEA), Cairo, Egypt

<sup>c</sup>Department of Food Chemistry and Biocatalysis, Wrocław University of Environmental and Life Sciences, Norwida 25, 50-375 Wrocław, Poland

<sup>d</sup>Department of Biochemistry, Faculty of Pharmacy, Ahran Canadian University (ACU), Giza, Egypt

<sup>e</sup>Department of Botany and Microbiology, College of Science, King Saud University, P.O. Box 2455, Riyadh 11451, Saudi Arabia

<sup>f</sup>Plant Production Department, College of Food and Agricultural Sciences, King Saud University, Saudi Arabia

<sup>g</sup>Department of Pharmaceutics, College of Pharmacy, King Saud University, Saudi Arabia

<sup>h</sup>Microbiology and Immunology Department, Faculty of Pharmacy, Ahran Canadian University (ACU), 6th October City, Giza, Egypt

<sup>i</sup>Botany and Microbiology Department, Faculty of Science, Al-Azhar University, Nasr City, Cairo 11884, Egypt. E-mail: amr.hosny86@azhar.edu.eg



healthy tissues, and they can also disseminate to different regions of the body *via* a phenomenon known as metastasis. Cancer can manifest in any anatomical region and has the potential to affect various organs and tissues. Cancer formation typically follows a complex series of genetic alterations that disrupt the normal control of cell growth and division.<sup>5</sup> These mutations can be acquired through exposure to specific risk factors, such as tobacco smoke, radiation, certain chemicals, infectious agents, and genetic predisposition, during an individual's lifespan. Nevertheless, it is crucial to acknowledge that not all cancers can be avoided, and certain types may arise without any identifiable risk factors.<sup>6</sup>

Traditional anticancer agents, also known as conventional chemotherapy, encompass a broad range of drugs that have been used for many years in cancer treatment. These agents are designed to kill or inhibit the growth of cancer cells by interfering with their ability to divide and multiply.<sup>7</sup> Cancer is a significant contributor to global mortality, with rising incidences observed on an annual basis.

The application of nanobiotechnology in pathogen resistance and fighting the cancer pandemic has demonstrated significant and robust outcomes in the fight against microbial infections and tumor treatment.<sup>8,9</sup> This is because the technology allows better attraction to the bacterial, fungal, and cancer cells and ROS production stimulates their inhibition.<sup>10,11</sup> Entire biological components have been included in the scope of biological methods for nanoparticles and nanocrystal production.<sup>12–15</sup> Due to its safety and environmental friendliness, the biological production of metal nanoparticles utilizing macromolecules, plants, bacteria, and fungi has drawn a lot of attention recently.<sup>8,16–22</sup>

Natural polymeric cap agents, such as chitosan and gum Arabic, are used to regulate the inorganic polymer NPs' particle size and improve their stability.<sup>23,24</sup> Gum Arabic is different from other macromolecules in biology in that it has a variety of attractive features that make it a preferred option for the production of nanomaterials. These crucial attributes are lower toxicity, biological compatibility, affordability, and availability.<sup>25</sup>

Bimetallic nanomaterials are receiving a lot of attention because of the distinctive chemical, physical, and physiological characteristics that result from the combination of several metal elements.<sup>24,26–29</sup> Copper oxide–zinc oxide (CuO–ZnO) NPs are the most well-known bimetallic nanoparticles (NPs) because of their chemically controllable plasmonic properties and prospective uses in the detection, catalysis, and combating microbial plant pathogens.<sup>27,30</sup> Throughout the review literature,<sup>24,26–28,31–34</sup> the produced bimetallic nanoparticles have shown encouraging antibacterial and antibiofilm action *versus* a particular category of extremely pathogenic and multidrug-resistant pathogens.

The bimetallic nanoparticles' electrostatic interaction, which attaches proteins to interfere with homeostasis (disturbing the chain of electron transport), inhibits signal transduction, harms the membranes of cells, interferes with enzymes and proteins, creates reactive oxygen species, also known as ROS,

and oxidative stress, and causes genotoxicity, may be involved in the mechanism of action of antimicrobials.<sup>35,36</sup>

In addition to their biological properties as antibacterial, antifungal and anticancer agents, the characterization of the synthesized bimetallic GA@CuO–ZnO NPs and one of the environmentally friendly methods for their production are the main topics of this study. GA@CuO–ZnO NPs may be prepared using a range of chemical, biological, and physical methods because of the remarkable progress in nanotechnology. Therefore, the purpose of this study was to synthesize and characterize a novel nanocomposite (GA@CuO–ZnO) and to assess its anticancer, antibacterial and antifungal activities.

## Materials and methods

### Chemicals and reagents

Analytical-grade chemicals, including gum Arabic (Meron Company, India), and zinc acetate and copper acetate (Sigma Aldrich, UK) were used for the production of bimetallic nanoparticles in the study.

### Synthesis of GA@CuO–ZnO nanocomposite

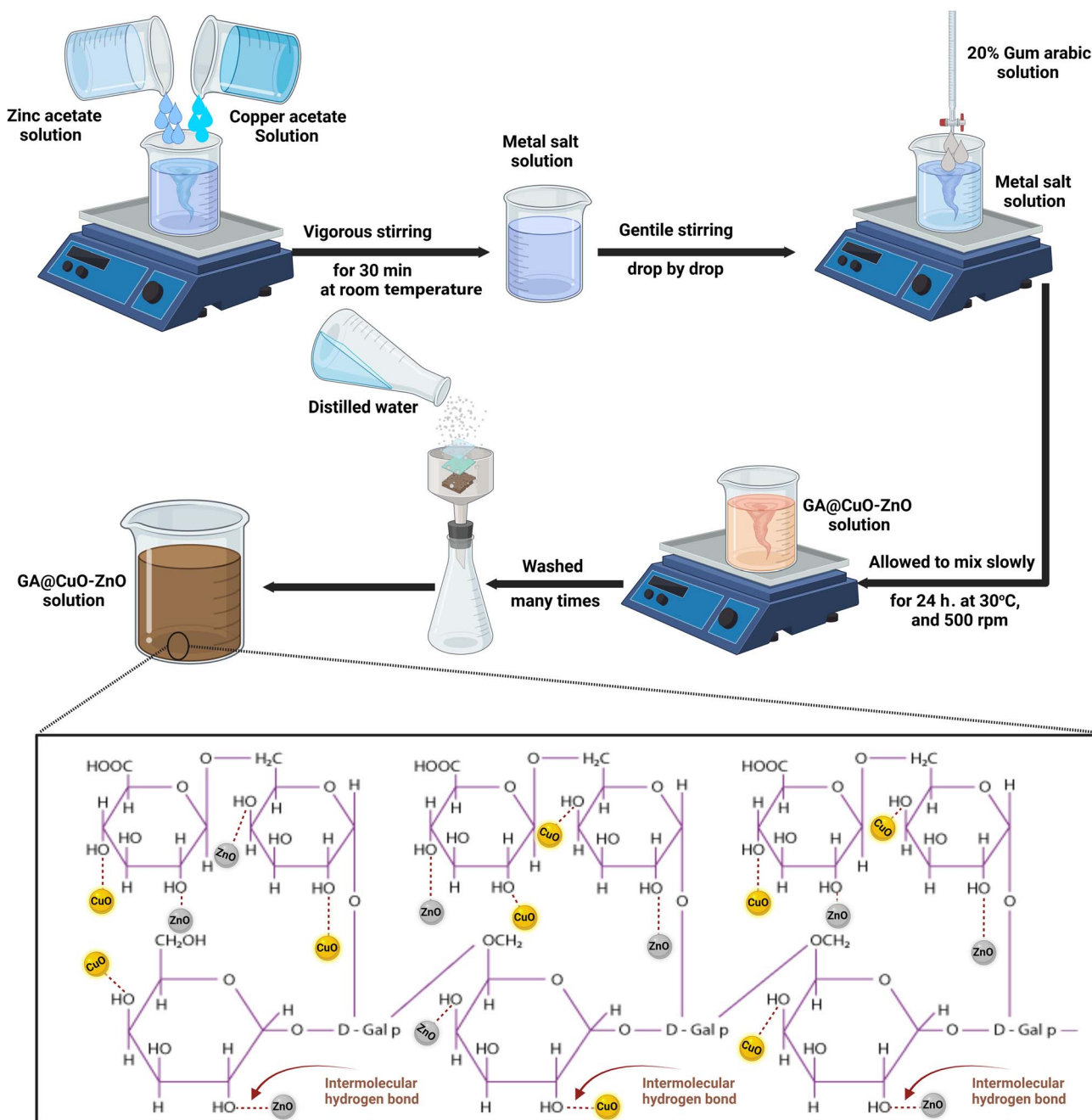
The precise amounts of the salts were employed in the biosynthesis of the nanocomposite. Specifically, 10 ml of (2.0 mM) Zn ( $\text{CH}_3\text{COO}$ )<sub>2</sub>(H<sub>2</sub>O)<sub>2</sub> and 10 ml of (2.0 mM) Cu( $\text{CH}_3\text{COO}$ )<sub>2</sub> (2.0 mM) were combined at room temperature for half an hour. After that, they received around 80 milliliters of the 20% gum Arabic that serves as a reducing and stabilizing agent. After combining the two solutions, the combination's pH was 7.8. To achieve the most effective synthesis of GA@CuO–ZnO nanocomposite, the reaction conditions were chosen to include a temperature-controlled incubation at 30 °C and a reaction duration of 24 h under agitation (500 rpm) in a shaking incubator, as shown in Scheme 1.<sup>37</sup>

According to the literature,<sup>24</sup> FTIR results revealed peak absorption values at 3291 cm<sup>−1</sup> (attributed to –OH), 2985 cm<sup>−1</sup> (symmetric and asymmetric –CH vibration), 1642 cm<sup>−1</sup> (attributed to –COOH), 1462 cm<sup>−1</sup> (uronic acid symmetrically stretched by carboxylic groups), 1066 cm<sup>−1</sup> (perhaps due to arabinogalactan), and 890.0 cm<sup>−1</sup> (attributed to galactose 1–4 linkage and mannose 1–6 linkage). The same peaks in the metal NPs spectra indicate that GA was successful in capping. Moreover, the galactose/mannose peak became less prominent and the arabinogalactan peak lost its doublet. Additionally, a clear peak at 715.25 cm<sup>−1</sup> was seen, which may be the outcome of metal NPs interacting and combining with hydroxyl groups to create metal–O.<sup>38</sup>

According to the results of El-Batal *et al.*,<sup>24</sup> all of the peaks were in identical wavenumbers, suggesting that the synthesized NPs were similarly incorporated and/or conjugated through the primary functional groups of the stabilizer GA. The lack of noise and additional unidentified peaks indicated the high purity of the synthesized sample.<sup>39</sup>

UV-Vis spectroscopy was used to compute the optical density (OD) of GA@CuO–ZnO nanocomposite at a given wavelength in order to ascertain the likelihood of the preparation.





Scheme 1 Schematic for the synthesis of GA@CuO-ZnO nanocomposite and the possible binding sites in GA.

### Characterization of the synthesized GA@CuO-ZnO nanocomposite

A UV-Vis spectrophotometer (JASCO V-560) was used to examine the absorbance and spectral properties of the produced GA@CuO-ZnO nanocomposite at particular wavelengths. An extra experiment devoid of any metal ions was offered for Auto-zero reasons. First, each specimen's optical characteristics were examined to ascertain the overall number of wavelengths required to estimate absorbance.

The mean size distribution of the prepared GA@CuO-ZnO nanocomposite was determined using the dynamic light

scattering measurements on a DLS-PSS-NICOMP 380-ZLS particle-sized system (St. Barbara, California, USA). A tiny cuvette was used to contain 100  $\mu\text{L}$  of the tested GA@CuO-ZnO nanocomposite. Following 2 min of equilibrium at  $25.0 \pm 2^\circ\text{C}$  ambient temperature, five procedures were carried out.

The generated GA@CuO-ZnO nanocomposite was further evaluated through a high-resolution transmission electron microscope (HR-TEM, JEM2100, JEOL, Japan) to determine their size, shape, and overall appearance. Furthermore, it was possible to examine the crystallization, crystallite diameters, and/or morphology of the generated GA@CuO-ZnO

nanocomposite by using the XRD-6000 instrument (Shimadzu equipment, and SSI, Japan). The produced GA@CuO-ZnO nanocomposite surrounding GA was analyzed utilizing a scanning electron microscope (SEM, ZEISS, EVO-MA10, Germany) to assess their surface form and arrangement. Finally, the surface charges of the produced GA@CuO-ZnO nanocomposite were informally evaluated at the pH of preparation using a zeta potential analyzer from Malvern Device, UK.<sup>40</sup>

### Antibacterial and antifungal activity

Antibacterial activity of the synthesized GA@CuO-ZnO nanocomposite was evaluated toward *Escherichia coli* ATCC 25922, *Salmonella typhimurium* ATCC 14028, *Staphylococcus aureus* ATCC 25923, *S. epidermis* ATCC 14990 and *Bacillus subtilis* ATCC 6051. Furthermore, antifungal activity was assessed against *Candida albicans* ATCC 90028, *Cryptococcus neoformans* ATCC14116, *Aspergillus fumigatus* ATCC 204305 and *A. brasiliensis* ATCC 16404. All steps of the agar well diffusion method were performed in strict adherence to CLSI document M51-A2.<sup>41</sup>

100  $\mu$ L of the synthesized GA@CuO-ZnO nanocomposite, zinc acetate, copper acetate, standard antibiotic (ampicillin/sulbactam; SAM 20), and antifungal drug (amphotericin B) were placed in agar wells (7 mm) seeded with bacterial and fungal strains separately, and then incubating at 37 °C for 24 h for bacterial and unicellular fungal strains, and at 30 °C for 72 h for filamentous fungal strains. After the incubation process, the inhibition zone for each treatment was measured,<sup>42–44</sup> and MIC was determined using the microdilution method.<sup>45–47</sup>

### Cytotoxicity and anticancer activity

Cytotoxicity of the synthesized GA@CuO-ZnO nanocomposite was evaluated according to the MTT protocol.<sup>48,49</sup> To check the biosafety of the synthesized GA@CuO-ZnO nanocomposite, a Wi38 normal cell line was used. Moreover, both MCF7 and HepG2 cancerous cell lines were used to assess the anticancer activity of the synthesized GA@CuO-ZnO nanocomposite. The optical density was measured at 560 nm. To determine cell viability, the following formula was used (1), and to determine cell inhibition, eqn (2) was applied:

$$\text{Viability}\% = \frac{\text{test OD}}{\text{control OD}} \times 100 \quad (1)$$

$$\text{Inhibition}\% = 100 - \text{viability}\% \quad (2)$$

## Results and discussion

### Synthesis and characterization of the synthesized GA@CuO-ZnO nanocomposite

Gum Arabic's ability to create GA@CuO-ZnO nanocomposite as a capping and reducing agent was assessed. When the bimetallic GA@CuO-ZnO nanocomposite was produced, the resulting solution's initially pale-yellow color was turned into a brown hue. The resulting brown color was attributed to the activation of the surface plasmon resonance that occurs within the

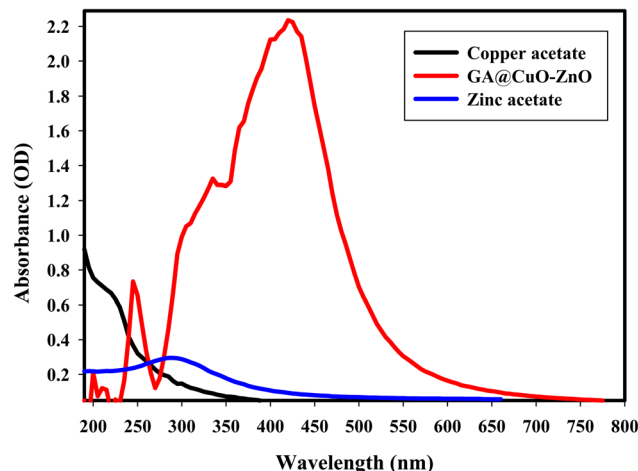


Fig. 1 UV-Vis spectra of copper acetate, zinc acetate, and the synthesized GA@CuO-ZnO nanocomposite.

GA@CuO-ZnO nanocomposite, and the change in particle size which provides a reliable spectroscopic indicator of their presence.<sup>50</sup>

The detected absorbance of 2.23 created the experimental peak in the spectra (Fig. 1), and the UV-Vis studies showed that the generated GA@CuO-ZnO nanocomposite was small and had a visible absorption peak at 420 nm. Conversely, Fig. 1 shows the UV-Vis spectra of the initial precursors, zinc acetate and copper acetate, which had distinct wavelengths; zinc acetate at 290 nm (ref. 51) and copper acetate at 210 nm.<sup>52</sup> It must be emphasized that a noted peak at 245 nm in the synthesized GA@CuO-ZnO nanocomposite spectrum corresponds to the GA spectrum.<sup>53</sup>

The intensity of the brown hue correlated with the ability for the biosynthesis of CuO-ZnO NPs that were generated.<sup>54</sup> Surface Plasmon resonance (SPR) is often influenced by the intensity, size, morphology, structure, and dielectric characteristics of any produced nanoparticles.<sup>55,56</sup>

The peak spectra generated for the synthesized GA@CuO-ZnO nanocomposite are broad, ranging from 270 to 500 nm, this is due to the formation of poly-dispersed GA@CuO-ZnO nanocomposite and other factors such as particle size distribution, and polydispersity index (PDI) (according to the result of DLS), surface defects (SEM result), particle size variation (HRTEM result), or the nature of the bimetallic interaction (Scheme 1).

The synthesized GA@CuO-ZnO nanocomposite was characterized by its hydrodynamic diameter, particle size dispersion, and polydispersity index (PDI) using Dynamic Light Scattering (DLS) analysis. By comparing the collected data with HR-TEM investigations, we were able to establish the average size of the created nanoparticles.<sup>57</sup>

The HR-TEM image in Fig. 2a demonstrated that the produced GA@CuO-ZnO nanocomposite was bound to stabilizing gum Arabic and had a semi-spherical shape. Fig. 2b shows that the particles' sizes ranged from 18.34 nm to 90.45 nm, with a median diameter of  $50.28 \pm 1.5$  nm. The produced gum Arabic filtrate was rich in active functional





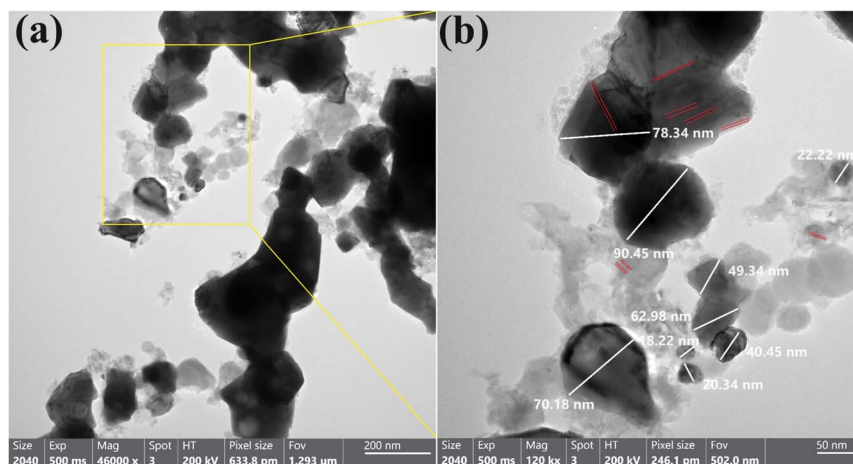


Fig. 2 HR-TEM images of the synthesized GA@CuO–ZnO nanocomposite (a), and their corresponding magnification (b).

groups and the supplied polydispersed NPs acted as capping agents, stabilizing, and reducing the concentration of these groups.<sup>58</sup> Zn and Cu may concurrently diminish due to the radical multilocation of gum Arabic, as elucidated and contrasted in our work. The HR-TEM image (Fig. 2b) demonstrated the uniform line spacing, which resulted in a single-grade system and copper was equally distributed throughout the zinc matrix, resulting in a unique alloy.<sup>24</sup>

Upon comparison with literature on average particle size and shape, our GA@CuO–ZnO nanocomposite was discovered to be polydispersed, with varying sizes and a preponderance of spherical particles. The NPs that were created had a spherical or orbicular shape, although the asymmetrical form could be due to the fact that they were created from green extract, which could have resulted in a variety of morphologies. Polydispersed NPs are a long-term solution since we used gum Arabic, the

most practicable reducing and covering agent, in our investigation.<sup>59</sup>

As shown in Fig. 3a, the usual size of the particle's dispersion for GA@CuO–ZnO nanocomposite, which was produced using gum Arabic, was determined using the DLS technique to be 80.34 nm. Samples are considered monodisperse according to the International Standards Organizations (ISOs) when the polydispersity index (PDI) readings are less than 0.05. Conversely, when PDI findings are more than 0.7, particles with a variable distribution are expected to be generated.<sup>60</sup> The PDI values of the GA@CuO–ZnO nanocomposite were 0.91, according to our findings. The prepared nanocomposite exhibited an acceptable polymorphism range according to the current values. Results demonstrated that HR-TEM imaging showed smaller particle estimations than the average and predominant sizes obtained by DLS analysis. According to the following citation,<sup>61</sup> the major factors contributing to the nanocomposite's enormous size are its internal hydrodynamic radius and the water layers immediately surrounding it. Fig. 3b shows the results of analyzing the GA@CuO–ZnO nanocomposite's zeta potential at a pH of 7.8 in the preparation. This study shows that the zeta potential of the fabricated GA@CuO–ZnO nanocomposite remains negative at the investigated material's pH. Because gum Arabic has a negative electrical charge, the preparation's zeta potential in the neutral medium (pH 7.8) was  $-30.5$  mV, as shown in Fig. 3b.

Using scanning electron microscopy (SEM) the surface form and characteristics of the synthesized nanoparticles can be analyzed. Fig. 4a shows that the synthesized GA@CuO–ZnO nanocomposite surfaces seem clear when viewed in conjunction with the gum Arabic SEM data, and the generated gum Arabic also had the corresponding bright spherical particles. Gum Arabic, which resembles fused and capped illuminated NPs, successfully partitioned the GA@CuO–ZnO nanocomposite into its spheroidal particle component (Fig. 4b).

In contrast to previous studies on the topic of morphological form, the synthesized GA@CuO–ZnO nanocomposite developed in this work exhibited uniform distribution, controlled size, and exact spherical shape. Mohsin *et al.*<sup>62</sup> synthesized bimetallic

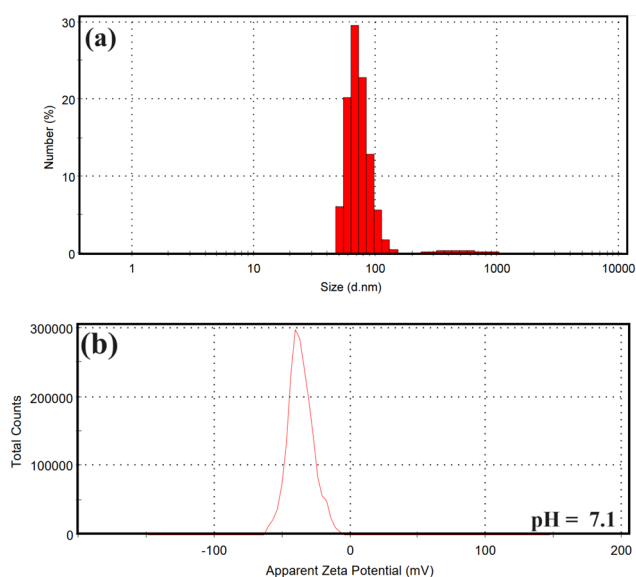


Fig. 3 Particle size distribution, and surface charge of the synthesized GA@CuO–ZnO nanocomposite: (a) DLS analysis, and (b) zeta potential.

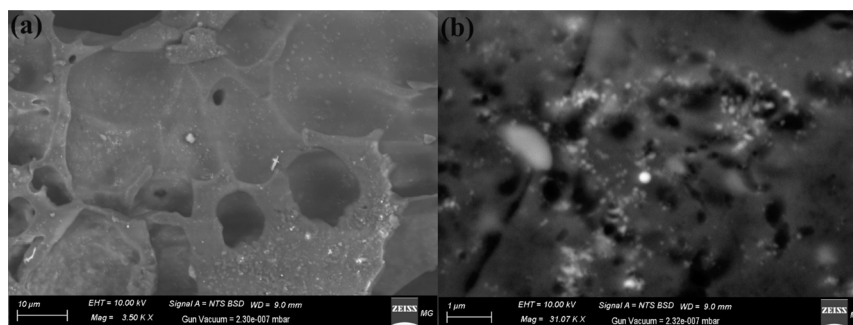


Fig. 4 SEM images of the synthesized GA@CuO–ZnO nanocomposite at different magnifications (a and b).

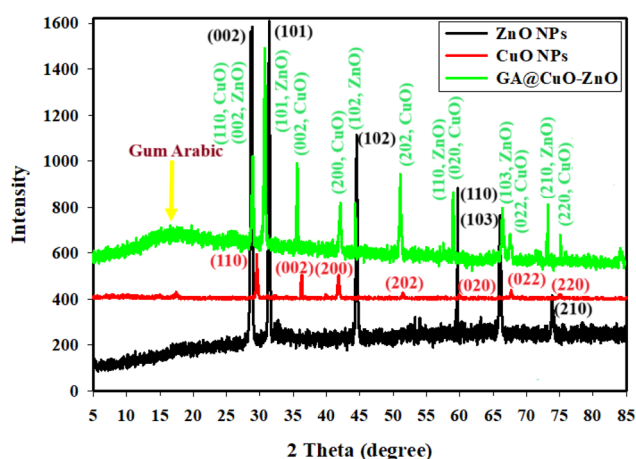


Fig. 5 XRD of the synthesized GA@CuO–ZnO nanocomposite, CuO NPs, and ZnO NPs.

silver and gold core-shell NPs by varying the pH and temperature settings of the citrate reduction process. The synthetic process is heavily dependent on pH and temperature because the approved morphological shape and border size specifications stipulate that the particles should appear spheroidal and maintain a size range of 50 to 65 nm.

Fig. 5 shows the results of XRD analyses conducted on a synthetic GA@CuO–ZnO nanocomposite. Both amorphous and crystalline structures are present in the final nanocomposite. In order to quickly identify the distinctive properties of the manufactured GA@CuO–ZnO nanocomposite, we analyze the XRD data of our newly produced ZnO NPs and CuO NPs as separate patterns (Fig. 5). It must be noted that  $2\theta$  represent the gum Arabic was in the exact range, which ranged from  $5^\circ$  to  $21^\circ$ .<sup>24</sup> Fig. 5 displays the XRD results of the produced bimetallic CuO–ZnO NPs and draws attention to the XRD diffraction peaks of the ZnO NPs. Using the standard card JCPDS number 36-1451, these peaks at  $2\theta = 27.40^\circ, 31.22^\circ, 45.54^\circ, 56.56^\circ, 67.17^\circ$ , and  $75.56^\circ$  correspond to Bragg's reflections at angles (002), (101), (102), (110), (103), and (201), respectively.<sup>63</sup>

Along with the typical card JCPDS number 89-2531, they additionally include the CuO NP diffraction peaks at  $2\theta = 30.22^\circ, 36.11^\circ, 40.75^\circ, 52.72^\circ, 58.27^\circ, 67.83^\circ$ , and  $71.45^\circ$ ; these peaks match Bragg's reflections at degrees (110), (002), (200), (020), (022), and (220),<sup>64</sup> respectively. There was

crystallization in the synthesized GA@CuO–ZnO nanocomposite, and the XRD data that was available showed that it had a face-centered cubic (fcc) crystal structure (Fig. 5). The production of highly crystalline bimetallic nanoparticles and their linking with amorphous gum Arabic, as confirmed from the XRD data, improved their dispersion in the solution and their potential use.<sup>65</sup>

Ultimately, the midway crystallite size of bimetallic CuO–ZnO NPs was determined using the Williamson–Hall (W–H) equation,<sup>66,67</sup> and it was found to be 29.46 nm.

$$\beta \cos \theta = \frac{k\lambda}{D_{W-H}} + 4\epsilon \sin \theta \quad (3)$$

### Antibacterial activity

In the current study, GA@CuO–ZnO nanocomposite and their starting materials were evaluated for antibacterial activity toward some pathogenic strains as shown in Table 1 and Fig. 6. Results revealed that GA@CuO–ZnO nanocomposite exhibited outstanding antibacterial activity against all tested bacterial strains. Table 1 illustrates the antibacterial activity of GA@CuO–ZnO nanocomposite where results showed that GA@CuO–ZnO nanocomposite exhibited antibacterial activity against *E. coli* and *S. typhimurium* as Gram-negative bacteria where inhibition zones were  $21 \pm 1.0$  and  $25.3 \pm 1.52$  mm, respectively, at a concentration of  $1000 \mu\text{g ml}^{-1}$ . Also, GA@CuO–ZnO nanocomposite showed antibacterial activity toward *B. subtilis*, *S. aureus* and *S. epidermis* as Gram-positive bacteria where inhibition zones were  $21.4 \pm 1.53$ ,  $23.5 \pm 1.80$  and  $24.4 \pm 0.57$  mm, respectively, at a concentration  $1000 \mu\text{g ml}^{-1}$ . Standard antibiotic SAM 20 exhibited weak antibacterial activity toward *S. typhimurium* and *S. aureus* only, but did not show any activity on other bacterial strains. Also, copper acetate and zinc acetate did not exhibit antibacterial activity toward all tested bacterial strains as the tested strains are multidrug-resistant (Fig. 6).

Furthermore, MICs of the GA@CuO–ZnO nanocomposite against all tested bacterial strains were evaluated, where the results revealed that the MIC of bimetallic CuO–ZnO NPs toward all strains was  $62.5 \mu\text{g ml}^{-1}$  except for *S. typhimurium* it was  $31.25 \mu\text{g ml}^{-1}$ . Turabik *et al.*<sup>68</sup> reported that bimetallic Cu/Zn NPs showed antibacterial activity where MIC was in the range of 16 and  $256 \mu\text{g ml}^{-1}$ . Additionally, *Cissus quadrangularis*



**Table 1** Inhibition zones and MICs of GA@CuO–ZnO nanocomposite against bacterial strains

Bacterial strain	Cu acetate IZ (mm)	Zn acetate IZ (mm)	GA@CuO–ZnO nanocomposite		SAM 20 IZ (mm)
			IZ (mm)	MIC ( $\mu\text{g ml}^{-1}$ )	
<i>E. coli</i>	ND	ND	$21 \pm 1.0^b$	62.5	ND
<i>S. typhi</i>	ND	ND	$25.3 \pm 1.52^a$	31.25	$16.0 \pm 0.60^a$
<i>B. subtilis</i>	ND	ND	$21.4 \pm 1.53^b$	62.5	ND
<i>S. aureus</i>	ND	ND	$23.5 \pm 1.80^{ab}$	62.5	$14.13 \pm 0.32^b$
<i>S. epidermis</i>	ND	ND	$24.4 \pm 0.57^{ab}$	62.5	ND

Data within the groups are analyzed using a one-way analysis of variance (ANOVA) followed by <sup>a,b</sup> Duncan's multiple range test (DMRT).

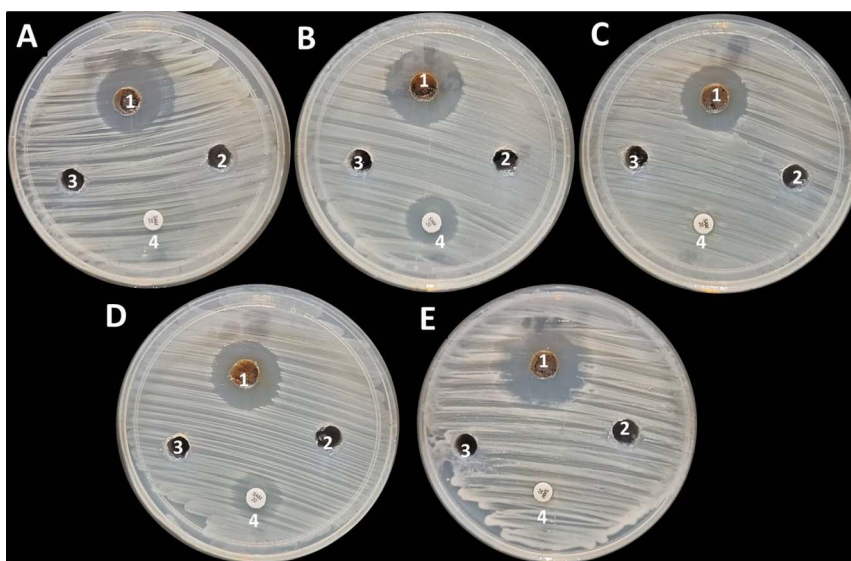


**Fig. 6** Antibacterial activity of GA@CuO–ZnO nanocomposite (1), copper acetate (2), zinc acetate (3) and SAM 20 (4) toward *E. coli* (A), *S. typhimurium* (B), *B. subtilis* (C), *S. aureus* (D), and *S. epidermis* (E).

stem was used for the synthesis of bimetallic Cu–Zn NPs, where results illustrate that it exhibited antibacterial activity against *E. coli* (MTCC-5704), *P. aeruginosa* (MTCC-2295), *B. subtilis* (MTCC-121), *S. aureus* (MTCC-3160) and *Streptococcus mutans* (MTCC-497).<sup>69</sup> Furthermore, in other study, bimetallic Zn–CuO NPs based nanocomposite was prepared, and exhibited high antibacterial activity toward *E. coli*, *S. aureus* and *B. subtilis* with MICs measured as 7.81 and 62.5  $\mu\text{g ml}^{-1}$ , respectively.<sup>30</sup>

When GA@CuO–ZnO nanocomposite interacts with cells, they can engage in electrostatic interactions with the cell membrane. This can lead to damage to the cell membrane, compromising its integrity and functionality. Disruption of the cell membrane can result in the leakage of the cellular components and ions, which can have detrimental effects on cellular processes. Moreover, the GA@CuO–ZnO nanocomposite can disrupt proteins and enzymes within the cells. Proteins play critical roles in various cellular processes, and their disruption can lead to malfunctioning of these processes. Enzymes, in particular, are essential for catalyzing biochemical reactions, and their disruption can interfere with metabolic pathways.

The formation of reactive oxygen species (ROS) is yet another effect that occurs as a result of the interaction between the GA@CuO–ZnO nanocomposite and different types of cells. ROS are chemicals that are extremely reactive and have the potential to contribute to oxidative stress within cells. There is a possibility that oxidative stress will cause damage to cellular components such as DNA, proteins, and lipids, which may ultimately result in cellular malfunction or even cell death. Furthermore, GA@CuO–ZnO nanocomposite has the ability to bind to proteins. This binding can disturb cellular homeostasis by interfering with normal protein functions. One example is the disruption of the electron transport chain, which is a crucial process for generating energy in cells. Interference with the electron transport chain can impair cellular respiration and overall energy production.<sup>35,36</sup>

#### Antifungal activity

The antifungal activity of GA@CuO–ZnO nanocomposite against both unicellular and multicellular fungi was assessed, as shown in Fig. 7. Results revealed that GA@CuO–ZnO





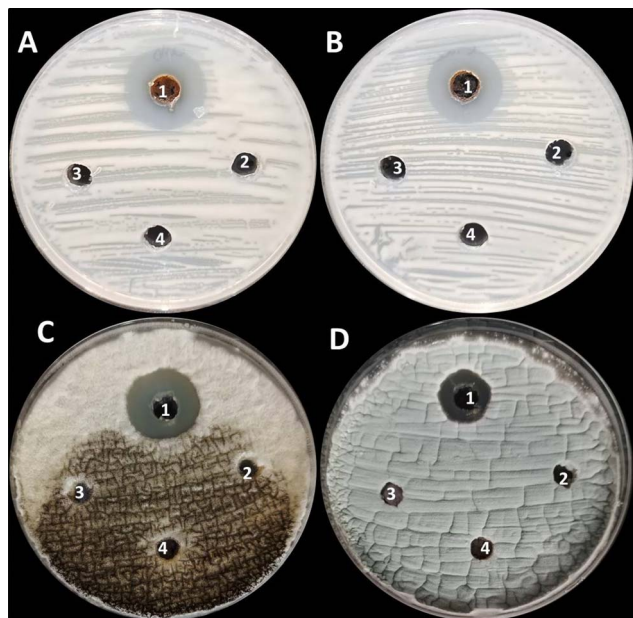


Fig. 7 Antifungal activity of GA@CuO-ZnO nanocomposite (1), copper acetate (2), zinc acetate (3) and amphotericin B (4) toward *C. albicans* (A), *C. neoformans* (B), *A. niger* (C) and *A. fumigatus* (D).

nanocomposite showed antifungal activity toward all tested fungal strains. Moreover, the GA@CuO-ZnO nanocomposite showed antifungal activity toward *C. albicans*, *C. neoformans* and *A. niger* with inhibition zones of  $23.86 \pm 1.60$ ,  $21.96 \pm 1.05$  and  $21.16 \pm 1.25$  mm, respectively, but showed weak antifungal activity toward *A. fumigatus* where inhibition zone was  $15.3 \pm 1.27$  mm (Table 2).

Furthermore, MICs of GA@CuO-ZnO nanocomposite against all tested fungal strains were tested. Results in Table 2 illustrated that the MIC of GA@CuO-ZnO nanocomposite toward all tested fungal strains was  $31.25 \mu\text{g ml}^{-1}$  except for *A. fumigatus* it was  $125 \mu\text{g ml}^{-1}$ . In a previous study, bimetallic copper-zinc nanoparticles exhibited significant antifungal activity toward *C. parapsilosis* and *C. tropicalis* with MICs of 32 and  $64 \mu\text{g ml}^{-1}$ , respectively.<sup>68</sup> Also, the nanocomposite based on bimetallic zinc-copper oxide nanoparticles showed weak antifungal activity with MIC  $250 \mu\text{g ml}^{-1}$  against *C. neoformans* and *C. albicans*.<sup>30</sup>

Gaber *et al.*<sup>22</sup> synthesized bimetallic CuO-ZnO NPs using *Aspergillus fumigatus* where it exhibited antifungal activity

toward *Fusarium oxysporum* with MIC of  $125 \mu\text{g ml}^{-1}$ . Gaber *et al.*<sup>22</sup> examined the impact of bimetallic ZnO-CuO on *F. oxysporum* using TEM ultrastructure analysis. They observed a complete destruction of all cellular components, disintegration of the cell wall, and damage to the plasma membrane. Furthermore, the nucleus exhibited a diminutive size and a distorted shape, while the chromatin components were dispersed throughout the cytoplasm, accompanied by many intensely pigmented bodies.

### Cytotoxicity and anticancer activity

In order to assess the safety of the produced compounds, it is essential to evaluate their cytotoxicity towards normal cell lines. The present work evaluated the cytotoxic effect of GA@CuO-ZnO nanocomposite on the normal cell lines Wi38 and Vero, as depicted in Fig. 8A. Results revealed that the IC<sub>50</sub> of GA@CuO-ZnO nanocomposite toward Wi38 was  $143.3 \mu\text{g ml}^{-1}$ . Cell viability of Wi38 at concentrations 31.25 and  $62.5 \mu\text{g ml}^{-1}$  were 99.28 and 88.49% respectively. Moreover, the IC<sub>50</sub> of the GA@CuO-ZnO nanocomposite toward the Vero normal cell line was  $220.9 \mu\text{g ml}^{-1}$ . Therefore, the prepared GA@CuO-ZnO nanocomposite in this study can be considered safe for use, as it exhibits a non-cytotoxic classification when the IC<sub>50</sub> value exceeds  $90 \mu\text{g ml}^{-1}$ .<sup>70</sup>

Fig. 8B shows that the GA@CuO-ZnO nanocomposite exhibited promising anticancer activity toward MCF7 and HepG2 and the activity against HepG2 was greater than that against the MCF7 cell line. The GA@CuO-ZnO nanocomposite showed IC<sub>50</sub>s of 54.7 and  $79.2 \mu\text{g ml}^{-1}$  toward HepG2 and MCF7, respectively.

When leaf extract of *Artemisia abyssinica* was used for biosynthesis of bimetallic Zn-Cu NPs, and evaluated for anticancer activity, it was found that the Zn-Cu NPs had anticancer activity 89% at  $500 \mu\text{g ml}^{-1}$  with an IC<sub>50</sub> value of  $33.12 \mu\text{g ml}^{-1}$  toward MCF7 cell line.<sup>71</sup> Another study<sup>72</sup> demonstrated the successful synthesis of Ag-ZnO nanoparticles using an extract derived from *Chonemorpha grandiflora* leaves, the efficacy of these nanoparticles was evaluated on MCF7, HCT116, and A549 cell lines. Previously, laser ablation was utilized to synthesize ZnO-Ag nanoparticles<sup>73</sup> and their anticancer capabilities were evaluated against HCT116 and HeLa cancer cell lines. In their study, Pandiyan *et al.*<sup>74</sup> (2019) found that the nanocomposite (Ag-Au/ZnO) exhibited promising anticancer properties against HeLa cells, which are human cervical cancer cells.

Table 2 Antifungal activity of GA@CuO-ZnO nanocomposite against unicellular and multicellular fungi

Fungal strain	Cu acetate IZ (mm)	Zn acetate IZ (mm)	GA@CuO-ZnO nanocomposite		Amphotericin B IZ (mm)
			IZ (mm)	MIC ( $\mu\text{g ml}^{-1}$ )	
<i>C. albicans</i>	ND	ND	$23.86 \pm 1.60^a$	31.25	ND
<i>C. neoformans</i>	ND	ND	$21.96 \pm 1.05^a$	31.25	ND
<i>A. niger</i>	ND	ND	$21.16 \pm 1.25^a$	31.25	ND
<i>A. fumigatus</i>	ND	ND	$15.3 \pm 1.27^b$	125	ND

Data within the groups are analyzed using a one-way analysis of variance (ANOVA) followed by <sup>a,b</sup> Duncan's multiple range test (DMRT).





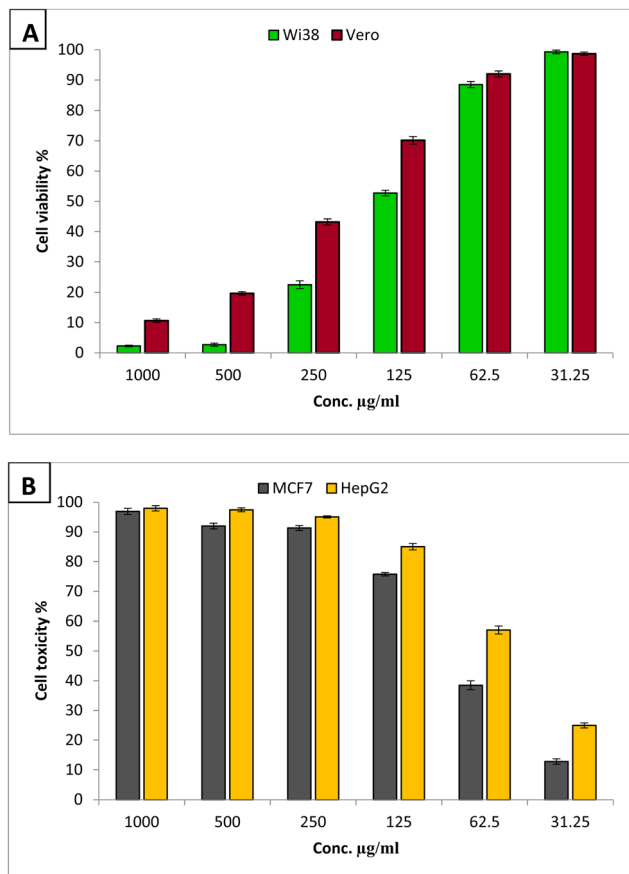


Fig. 8 Cytotoxicity of GA@CuO–ZnO nanocomposite against Wi38 and Vero normal cell lines (A), and anticancer activity against MCF7 and HepG2 cancerous cell lines (B).

Bimetallic nanoparticles can exhibit synergistic effects, where the combination of two metals enhances their individual anticancer activities. For example, the presence of multiple metals can lead to increased reactive oxygen species (ROS) generation, which can induce oxidative stress and subsequent cancer cell death. Also, bimetallic nanoparticles often possess improved stability and biocompatibility compared to individual metal nanoparticles. This allows for their effective delivery and interaction with cancer cells, leading to enhanced therapeutic efficacy.<sup>75</sup>

## Conclusions

In the current study, GA@CuO–ZnO nanocomposite was successfully synthesized through an eco-friendly green method. Characterization results revealed that the synthesized GA@CuO–ZnO nanocomposite showed a UV absorption peak at 420 nm, and was semi-spherical in shape with an average diameter of  $50.28 \pm 1.5$  nm. Antibacterial and antifungal activities were evaluated toward different microbial strains. The GA@CuO–ZnO nanocomposite showed significant antibacterial efficacy against both Gram-positive and Gram-negative bacteria. In addition, the GA@CuO–ZnO nanocomposite demonstrated antifungal properties against both single-celled and multi-

celled fungi. Furthermore, the safety of the GA@CuO–ZnO nanocomposite was established on the Wi38 normal cell line through cytotoxicity data. The  $IC_{50}$  value, which indicates the concentration at which 50% of the cells are affected, was found to be  $143.3 \mu\text{g ml}^{-1}$ . In addition, the GA@CuO–ZnO nanocomposite demonstrated significant potential in inhibiting the growth of MCF7 and HepG2 cancer cell lines, with  $IC_{50}$  values of 54.7 and  $79.2 \mu\text{g ml}^{-1}$ , respectively. Finally, the synthesized GA@CuO–ZnO nanocomposite using gum Arabic showed promising different biological activities, thus it can be used for combating pathogenic microbes and cancer in the medical field after extensive *in vivo* studies. One of the limitations of our work is that optimizing the synthetic process for NP synthesis was necessary to create extremely concentrated, small-sized bimetallic NPs. Our next work to validate the production of bimetallic CuO–ZnO NPs must involve numerous confirmations, including XPS and EDX analysis. This is necessary to establish the composition and assure repeatability of the synthesis procedure.

## Data availability

The datasets generated and analyzed during the current study are available from the corresponding author upon reasonable request.

## Author contributions

Gharieb S. El-Sayyad: conceptualization, methodology, writing – original draft preparation, writing – review and editing; El-Sayed R. El-Sayed: methodology, writing – original draft preparation; Samar H. Rizk: methodology, writing – original draft preparation; Mostafa A. Abdel-Maksoud: methodology, writing – original draft preparation; Adel M. Zakri: methodology, writing – review and editing, critically revising; Abdul Malik: methodology, writing – review and editing, critically revising; Mohamed N. Malash: methodology, writing – review and editing; Amr H. Hashem: conceptualization, methodology, writing – original draft preparation, writing – review and editing.

## Conflicts of interest

The authors declare that they have no conflict of interest.

## Acknowledgements

The authors extend their appreciation to King Saud University, Riyadh, Saudi Arabia, for Supporting Project number (RSP2025R376).

## References

- 1 F. Prestinaci, P. Pezzotti and A. Pantosti, *Pathog. Global Health*, 2015, **109**, 309–318.
- 2 L. M. Bebell and A. N. Muiru, *Glob. Heart*, 2014, **9**, 347–358.
- 3 M. A. Salam, M. Y. Al-Amin, M. T. Salam, J. S. Pawar and N. Akhter, *Healthcare*, 2023, **11**(13), 1946.



- 4 G. Muteeb and M. T. Rehman, *Pharmaceuticals*, 2023, **16**(11), 1615.
- 5 A. U. Khan, H. S. Dagur, M. Khan, N. Malik, M. Alam and M. Mushtaque, *Eur. J. Med. Chem. Rep.*, 2021, **3**, 100010.
- 6 M. Pandi, R. SenthilKumaran, P. Rajapriya, S. Yogeswari and J. Muthumary, *Biores. Bull.*, 2013, **2**, 1–9.
- 7 S. Dasari and P. B. Tchounwou, *Eur. J. Pharmacol.*, 2014, **740**, 364–378.
- 8 E. Saied, A. H. Hashem, O. M. Ali, S. Selim, M. S. Almuhayawi and M. A. Elbahnasawy, *Life*, 2022, **12**, 1331.
- 9 M. A. Albalawi, A. M. Abdelaziz, M. S. Attia, E. Saied, H. H. Elganzory and A. H. Hashem, *Antioxidants*, 2022, **11**, 2323.
- 10 J. M. Rajwade, R. Chikte and K. Paknikar, *Appl. Microbiol. Biotechnol.*, 2020, **104**, 1437–1461.
- 11 L. Fu, Z. Wang, O. P. Dhankher and B. Xing, *J. Exp. Bot.*, 2020, **71**, 507–519.
- 12 P. K. Tyagi, *Int. J. Curr. Microbiol. Appl. Sci.*, 2016, **5**, 548–558.
- 13 M. Abd Elkodous, H. M. El-Husseiny, G. S. El-Sayyad, A. H. Hashem, A. S. Doghish, D. Elfadil, Y. Radwan, H. M. El-Zeiny, H. Bedair and O. A. Ikhdair, *Nanotechnol. Rev.*, 2021, **10**, 1662–1739.
- 14 A. H. Hashem, E. Saied, O. M. Ali, S. Selim, S. K. Al Jaouni, F. M. Elkady and G. S. El-Sayyad, *Appl. Biochem. Biotechnol.*, 2023, **195**, 5753–5776.
- 15 M. Saied, M. Hasanin, T. M. Abdelghany, B. H. Amin and A. H. Hashem, *Int. J. Biol. Macromol.*, 2023, **242**, 124709.
- 16 N. H. Kamaruzaman, N. N. M. Noor, R. M. S. R. Mohamed, A. Al-Gheethi, S. K. Ponnusamy, A. Sharma and D.-V. N. Vo, *Environ. Res.*, 2022, **209**, 112831.
- 17 A. H. Hashem, T. A. Selim, M. H. Alruhaili, S. Selim, D. H. M. Alkhalifah, S. K. Al Jaouni and S. S. Salem, *J. Funct. Biomater.*, 2022, **13**, 112.
- 18 O. M. Ali, M. S. Hasanin, W. B. Suleiman, E. E.-H. Helal and A. H. Hashem, *Biomass Convers. Biorefin.*, 2024, **14**, 6987–6998.
- 19 E. Saied, S. S. Salem, A. A. Al-Askar, F. M. Elkady, A. A. Arishi and A. H. Hashem, *Bioengineering*, 2022, **9**, 397.
- 20 A. H. Hashem, E. Saied, B. H. Amin, F. O. Alotibi, A. A. Al-Askar, A. A. Arishi, F. M. Elkady and M. A. Elbahnasawy, *J. Funct. Biomater.*, 2022, **13**, 242.
- 21 A. H. Hashem, M. E. El-Naggar, A. M. Abdelaziz, S. Abdelbary, Y. R. Hassan and M. S. Hasanin, *Int. J. Biol. Macromol.*, 2023, **249**, 126011.
- 22 S. E. Gaber, A. H. Hashem, G. S. El-Sayyad and M. S. Attia, *Biomass Convers. Biorefin.*, 2024, **14**, 25395–25409.
- 23 M. G. Naseri, E. B. Saion, H. A. Ahangar and A. H. Shaari, *Mater. Res. Bull.*, 2013, **48**, 1439–1446.
- 24 A. I. El-Batal, M. Abd Elkodous, G. S. El-Sayyad, N. E. Al-Hazmi, M. Gobara and A. Baraka, *Int. J. Biol. Macromol.*, 2020, **165**, 169–186.
- 25 P. Chawla, N. Kumar, A. Bains, S. B. Dhull, M. Kumar, R. Kaushik and S. Punia, *Int. J. Biol. Macromol.*, 2020, **146**, 232–242.
- 26 R. R. El-Behery, E.-S. R. El-Sayed and G. S. El-Sayyad, *BMC Microbiol.*, 2023, **23**, 224.
- 27 M. S. Attia, G. S. El-Sayyad, A. M. Abdelaziz, S. E. Gaber, A. M. A. Khalil, A. M. Saleh, O. M. Al zoubi and A. H. Hashem, *Agronomy*, 2023, **13**, 2725.
- 28 A. H. Hashem, G. S. El-Sayyad, A. A. Al-Askar, S. A. Marey, H. AbdElgawad, K. A. Abd-Elsalam and E. Saied, *Plants*, 2023, **12**, 3288.
- 29 A. I. El-Batal, M. I. Eisa, M. A. M. Saad, H. M. Fakhry, W. M. El-Neshwy, S. S. Abdel-Fatah, F. M. Mosallam and G. S. El-Sayyad, *Int. J. Biol. Macromol.*, 2024, **262**, 130010.
- 30 M. S. Hasanin, A. H. Hashem, A. A. Al-Askar, J. Haponiuk and E. Saied, *Electron. J. Biotechnol.*, 2023, **65**, 45–55.
- 31 A. H. Hashem and G. S. El-Sayyad, *Biomass Convers. Biorefin.*, 2023, 1–13.
- 32 A. I. El-Batal, B. M. Al-shammari, G. S. El-Sayyad, S. H. Rizk, A. M. Abdelaziz, M. M. Nofel and M. S. Attia, *Biomass Convers. Biorefin.*, 2023, 1–18.
- 33 B. H. Elkhodary, M. S. Attia, G. S. El-Sayyad and M. S. Salem, *Biomass Convers. Biorefin.*, 2023, 1–24.
- 34 H. Y. Mostafa, G. S. El-Sayyad, H. G. Nada, R. A. Ellethy and E. Zaki, *Arch. Biochem. Biophys.*, 2023, **736**, 109539.
- 35 P. V. Baptista, M. P. McCusker, A. Carvalho, D. A. Ferreira, N. M. Mohan, M. Martins and A. R. Fernandes, *Front. Microbiol.*, 2018, **9**, 1441.
- 36 N. Arora, K. Thangavelu and G. N. Karanikolos, *Front. Chem.*, 2020, **8**, 412.
- 37 A. M. Saad, M. T. El-Saadony, A. M. El-Tahan, S. Sayed, M. A. Moustafa, A. E. Taha, T. F. Taha and M. M. Ramadan, *Saudi J. Biol. Sci.*, 2021, **28**, 5674–5683.
- 38 A. Ashour, A. I. El-Batal, M. A. Maksoud, G. S. El-Sayyad, S. Labib, E. Abdeltwab and M. El-Okr, *Particuology*, 2018, **40**, 141–151.
- 39 A. I. El-Batal, N. M. Balabel, M. S. Attia and G. S. El-Sayyad, *J. Cluster Sci.*, 2020, **31**, 1021–1040.
- 40 A. Said, M. Abu-Elghait, H. M. Atta and S. S. Salem, *Appl. Biochem. Biotechnol.*, 2023, 1–14.
- 41 W. Pa, *Reference method for broth dilution antifungal susceptibility testing of yeasts*, Approved standard, CLSI document M27-A2, Clinical and Laboratory Standards Institute, 2nd edn, 2002, <https://clir.nii.ac.jp/crid/1570854176048718848>.
- 42 A. M. Shehabeldine, A. H. Hashem, A. R. Wassel and M. Hasanin, *Appl. Biochem. Biotechnol.*, 2022, **194**, 783–800.
- 43 A. H. Hashem, M. Hasanin, S. Kamel and S. Dacrorry, *Colloids Surf., B*, 2022, **209**, 112172.
- 44 M. Hasanin, A. H. Hashem, A. A. El-Rashedy and S. Kamel, *Cellulose*, 2021, **28**, 8355–8374.
- 45 C. Valgas, S. M. D. Souza, E. Smânia and A. Smânia, *Braz. J. Microbiol.*, 2007, **38**, 369–380.
- 46 A. H. Hashem, A. M. A. Khalil, A. M. Reyad and S. S. Salem, *Biol. Trace Elem. Res.*, 2021, 1–11.
- 47 A. H. Hashem, A. M. Shehabeldine, A. M. Abdelaziz, B. H. Amin and M. H. Sharaf, *Appl. Biochem. Biotechnol.*, 2022, **194**, 3468–3482.
- 48 A. Van de Loosdrecht, R. Beelen, G. Ossenkoppele, M. Broekhoven and M. Langenhuijsen, *J. Immunol. Methods*, 1994, **174**, 311–320.



- 49 A. Khalil, A. Abdelaziz, M. Khaleil and A. Hashem, *Lett. Appl. Microbiol.*, 2021, **72**(3), 263–274.
- 50 M. Sui, S. Kunwar, P. Pandey and J. Lee, *Sci. Rep.*, 2019, **9**, 1–14.
- 51 A. A. Barzinjy and H. H. Azeez, *SN Appl. Sci.*, 2020, **2**, 991.
- 52 H. Rani, S. P. Singh, T. P. Yadav, M. S. Khan, M. I. Ansari and A. K. Singh, *Mater. Chem. Phys.*, 2020, **239**, 122052.
- 53 M. S. Attia, N. M. Balabel, I. M. Ababutain, M. S. Osman, M. M. Nofel, M. Abd Elkodous, W. F. Elkhatib, G. S. El-Sayyad and A. I. El-Batal, *J. Cluster Sci.*, 2022, **33**, 1373–1386.
- 54 R. Munir, K. Ali, S. A. Z. Naqvi, M. A. Maqsood, M. Z. Bashir and S. Noreen, *Sep. Purif. Technol.*, 2023, **306**, 122527.
- 55 K. L. Kelly, E. Coronado, L. L. Zhao and G. C. Schatz, *J. Phys. Chem. B*, 2023, **107**(3), 668–677.
- 56 K. S. Prasad and K. Selvaraj, *Biol. Trace Elem. Res.*, 2014, **157**, 275–283.
- 57 A. Lawrie, A. Albanyan, R. Cardigan, I. Mackie and P. Harrison, *Vox Sang.*, 2009, **96**, 206–212.
- 58 P. Monika, M. Chandraprabha, R. Hari Krishna, M. Vittal, C. Likhitha, N. Pooja and V. Chaudhary, *Biotechnol. Genet. Eng. Rev.*, 2022, 1–29.
- 59 E. Castro-Longoria, A. R. Vilchis-Nestor and M. Avalos-Borja, *Colloids Surf., B*, 2011, **83**, 42–48.
- 60 M. Nissen, R. Förster, T. Wieduwilt, A. Lorenz, S. Jiang, W. Hauswald and M. A. Schmidt, *Small*, 2022, **18**, 2202024.
- 61 T. G. Souza, V. S. Ciminelli and N. D. S. Mohallem, *J. Phys.:Conf. Ser.*, 2016, **733**, 012039.
- 62 M. Mohsin, M. Jawad, M. A. Yameen, A. Waseem, S. H. Shah and A. J. Shaikh, *Plasmonics*, 2020, **15**, 1599–1612.
- 63 F. Bigdeli and A. Morsali, *Mater. Lett.*, 2010, **64**, 4–5.
- 64 M. A. Siddiquee, M. ud din Parray, M. R. Kamli, M. A. Malik, S. H. Mehdi, K. Imtiyaz, M. M. A. Rizvi, H. K. Rajor and R. Patel, *J. Mater. Res. Technol.*, 2021, **13**, 2066–2077.
- 65 S. Poyraz, I. Cerkez, T. S. Huang, Z. Liu, L. Kang, J. Luo and X. Zhang, *ACS Appl. Mater. Interfaces*, 2014, **6**, 20025–20034.
- 66 P. Belavi, G. Chavan, L. Naik, R. Somashekar and R. Kotnala, *Mater. Chem. Phys.*, 2012, **132**, 138–144.
- 67 K. Pal, M. A. Elkodous and M. M. Mohan, *J. Mater. Sci.: Mater. Electron.*, 2018, **29**, 10301–10310.
- 68 M. Turabik, S. Özdemir, G. Akinbingol, S. Gonca and C. Geggel, *Inorg. Chem. Commun.*, 2023, **155**, 111072.
- 69 S. Khatak, N. Wadhwa and P. Jain, *Biosci., Biotechnol. Res. Asia*, 2021, **17**, 763–774.
- 70 J.-R. Ioset, R. Brun, T. Wenzler, M. Kaiser and V. Yardley, *A Training Manual for Screening in Neglected Diseases*, 2009.
- 71 T. A. Orshiso, E. A. Zereffa, H. C. A. Murthy, T. B. Demissie, O. Pardeshi, L. S. Avhad and S. Ghotekar, *ACS Omega*, 2023, **8**, 41039–41053.
- 72 N. Ambujakshi, H. Raveesha, S. Manohara, N. Dhananjaya, S. Pratibha and C. Shivakumara, *Mater. Res. Express*, 2019, **6**, 095068.
- 73 K. A. Elsayed, M. Alomari, Q. A. Drmosh, M. Alheshibri, A. Al Baroot, T. S. Kayed, A. A. Manda and A. L. Al-Alotaibi, *Alexandria Eng. J.*, 2022, **61**, 1449–1457.
- 74 N. Pandiyan, B. Murugesan, M. Arumugam, J. Sonamuthu, S. Samayanan and S. Mahalingam, *J. Photochem. Photobiol., B*, 2019, **198**, 111559.
- 75 H. Makada, S. Habib and M. Singh, *Sci. Afr.*, 2023, **20**, e01700.

